ACS Combinatorial Science

Research Article

pubs.acs.org/acscombsci

Combinatorial Study of the Li−Ni−Mn−Co Oxide Pseudoquaternary System for Use in Li−Ion Battery Materials Research

Colby R. Brown,[†] Eric McCalla,[†] Cody Watson,[†] and J. R. Dahn*[,†,∥]

[†]Department of Physics and [∥]Department of Chemistry, Dalhousie University, Halifax, Nova Scotia B3H 4R2, Canada

Supporting Information

ABSTRACT: Combinatorial synthesis has proven extremely effective in screening for new battery materials for Li−ion battery electrodes. Here, a study in the Li−Ni−Mn−Co−O system is presented, wherein samples with nearly 800 distinct compositions were prepared using a combinatorial and high-throughput method to screen for single-phase materials of high interest as next generation positive electrode materials. X-ray diffraction is used to determine the crystal structure of each sample. The Gibbs' pyramid representing the pseudoquaternary system was studied by making samples within three distinct pseudoternary planes defined at fractional cobalt metal contents of 10%, 20%, and 30% within the Li−Ni−Mn−Co−O system. Two large single-phase regions were observed in the system: the layered region (ordered rocksalt) and cubic spinel region; both of which are of interest for next-generation positive electrodes in lithium-ion batteries. These regions were each found to stretch over a wide range of compositions within the Li−Ni−Mn−Co−O pseudoquaternary system and had complex coexistence regions existing between them. The sample cooling rate was found to have a significant effect on the position of the phase boundaries of the single-phase regions. The results of this work are intended to guide further research by narrowing the composition ranges worthy of study and to illustrate the broad range of applications where solution-based combinatorial synthesis can have significant impact.

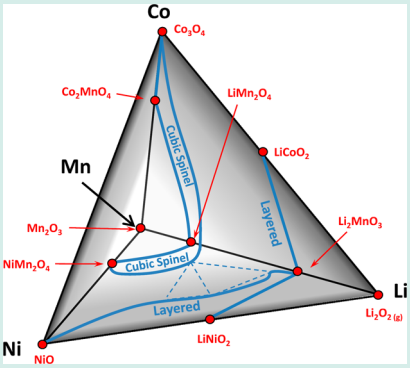

KEYWORDS: *Li−ion cathode, single-phase materials, cubic spinel, layered lithium transition metal oxides, combinatorial synthesis, X-ray diffraction*

INTRODUCTION

Lithium (Li)−ion batteries are currently the most widely used rechargeable energy storage devices in the world and their high demand is expected to grow in the coming decades.[1] To meet the growing performance demand imposed on Li−ion batteries for applications such as off-grid energy storage and electric vehicles, electrode materials combining a high energy density with high charge and discharge rate capabilities are required. Positive electrode materials account for roughly 1/3 the total cost of the Li−ion cell and strongly influence its electrochemical performance.[1,2] The positive electrode is therefore a crucial component to upgrade to improve the performance and lower the cost of future Li−ion cells.

Our work applies a combinatorial approach originally developed by Carey and Dahn to find composition regions of interest for Li−ion positive electrode materials.[3] Many current commercialized Li−ion cathode materials, such as $LiCoO_2$, $LiNi_{1/3}Mn_{1/3}Co_{1/3}O_2$, and $LiMn_2O_4$, all lie within the Li−Ni−Mn−Co−O system. The work presented here investigates the Li−Ni−Mn−Co−O system for samples with cobalt contents of 10%, 20%, and 30% of overall metal content that were heated to 800 °C under oxygen and subsequently cooled by quenching or regular-cooling. Figure 1 illustrates the sections of the Li−Ni−Mn−Co−O pseudoquaternary system targeted by the current work. The red triangles highlight pseudoternary planes defined at the cobalt fractional metal contents of 10%, 20%, and 30% within the pseudoquaternary system. These ternary planes will be referred to as "cobalt slices" from this point forward. The objective of this work is to expand on the work by McCalla et al., where the Li−Ni−Mn−O system (no Co) was studied,[4,5] by mapping the entire single-phase regions existing at low cobalt content within the Li−Ni−Mn−Co−O system. Single-phase positive electrode materials are desirable, as they provide better electrochemical performance when compared to multiphase materials.[6] Furthermore, single-phase positive electrode materials of compositions situated near boundaries to single-phase regions tend to provide the best electrochemical performances overall.[6] The materials investigated in the work presented here were characterized only by structure and no electrochemical analysis was performed. The single-phase composition regions of interest in the Li−Ni−Mn−Co−O system determined by this work are intended to identify composition regions that warrant further electrochemical study.

The most studied compositions within the Li−Ni−Mn−Co−O system that contain all four metals are often referred to in the literature as "NMC" materials, which are of the form $Li[Ni_xMn_yCo_{1-x-y}]O_2$ and the most commonly promoted NMC material in the literature is $LiNi_{1/3}Mn_{1/3}Co_{1/3}O_2$.[7−9] The proposed benefits of layered NMC materials over more

Received: March 24, 2015
Published: May 13, 2015

DOI: 10.1021/acscombsci.5b00048
ACS Comb. Sci. 2015, 17, 381−391

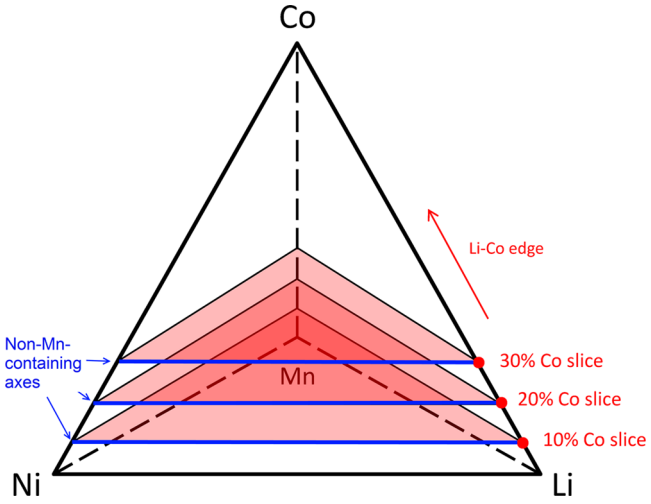

Figure 1. Illustration of the cobalt slice ternary phase diagrams existing within the Li−Ni−Mn−Co−O pseudoquaternary phase system defined at 10%, 20%, and 30% cobalt fractional metal content. The Li−Co edge and the non-Mn-containing axis of each pseudoternary plane are labeled in red and blue respectively, and will be referenced in the text.

common materials such as $LiCoO_2$ are a lower cost, lower toxicity, better thermal stability when charged, higher reversible capacity (if charged to high potential like 4.5 V), and better stability when cycling at elevated temperatures.[6] There is also much interest in high-capacity Li-rich positive electrode materials currently and recent work seems promising for improving the irreversible capacity of these materials.[10] However, these materials still experience significant amounts of voltage fade during cycling, which reduces total cell capacity during cycling.[11] If the voltage fade of these Li-rich materials were to be minimized in combination with low irreversible capacity then these materials could prove to be highly useful in the future.

There is also intense interest in various single-phase layered compounds as well as spinel-layered core−shell materials synthesized with low Co content.[2,7−9,12] Lower cobalt content materials are desirable since Co is significantly the most expensive element compared to Li, Ni, and Mn, and Co is also toxic for the environment. The results of the current work should prove useful for researchers investigating such positive electrode materials.

EXPERIMENTAL PROCEDURES

Combinatorial arrays of milligram-scale samples belonging to the Li−Ni−Mn−Co−O pseudoquaternary system were produced following the combinatorial methods described in detail elsewhere.[3,4,13,14] A Cartesian Pixsys solution-processing robot was used to dispense arrays of combinatorial samples onto alumina plates (Pi-Kem, 96%) that were previously coated with stearic acid (Aldrich, 96%). Ammonium bicarbonate (Alfa Aesar, 98%) was added in order to induce coprecipitation of mixed-metal carbonates in each sample. All samples were heated to 800 °C for 3 h under a flow of oxygen in order to form the oxide structure while minimizing lithium loss.[14] Heated samples were subsequently cooled by either placing the alumina plate sample holders directly onto an iron slab (quenching) or turning power to the furnace off (regular-cooling). The quenching cooling rate was measured to be roughly 10 °C/sec using an infrared temperature sensor while the regular-cooled rate was observed to be roughly 10 °C/min on average.

Figure 2 shows all targeted compositions within the cobalt slices of the Li−Ni−Mn−Co−O pseudoquaternary system for both quenched and regular-cooled samples. Nearly 800 unique compositions were synthesized to map the phase regions of the 10%, 20%, and 30% cobalt slice ternary phase diagrams within the Li−Ni−Mn−Co−O system. The cobalt slices shown in Figure 2 were each mapped by at least 99 distinct compositions, which are represented by blue dots for quenched and red dots for regular-cooled samples, respectively. Furthermore, the regular-cooled 10% cobalt slice (shown in Figure 2 f) had two additional series prepared to closely investigate the single-phase cubic spinel and layered regions observed there.

After synthesis, the metal oxide combinatorial samples were transferred onto a silicon oxide substrate and characterized using a Bruker D8 Discover X-ray diffractometer that used Cu−Kα radiation collimated to a 0.5 mm wide beam, a Göbel mirror, and an area X-ray detector. Each XRD pattern was constructed from three acquisition frames that had 30% overlap with one another. Samples were translated through a 1 mm × 1 mm area during XRD measurements in order to maximize the reflections observed from the small combinatorial samples. Each XRD pattern was acquired over a 2θ range of 15 to 70° with a step size of 0.02°. In-house software was used to fit the XRD patterns and extract lattice parameters for both single-phase and multiphase samples as described previously.[4,14]

The metal content of a select few samples synthesized during this work were determined by ICP-OES. To perform these measurements on combinatorial samples, each sample had to be manually transferred into individual vials using a stainless steel scapula that was cleaned with isopropyl alcohol between each transfer in order to prevent sample contamination. Approximately 0.5 mL of prepared aqua regia solution (25% HNO_3, 75% HCl) was added to each vial in order to dissociate the metals from their metal oxide compounds. The high cost per-sample of ICP elemental analysis prevented being able to measure compositions for the majority of combinatorial samples prepared in this work. However, the metal concentrations of all sample-dispensing solutions were measured three separate times to obtain concentrations accurate to an error of 3%. Because of the high precision of the solutions-processing robot used to dispense every combinatorial sample, the 3% error in metal concentration of the dispensing solutions was assumed to be the main source of error in the dispensed compositions.

RESULTS AND DISCUSSION

Figure 3 shows the resulting series of cobalt slice phase diagrams corresponding to quenched samples and Figure 4 shows the resulting series of cobalt slice phase diagrams corresponding to regular-cooled samples in the Li−Ni−Mn−Co−O pseudoquaternary system. It is not trivial to locate common compositions in these diagrams. Therefore, Figures 3 and 4 also show the positions of some examples of the NMC class of materials described in the Introduction: $Li[Ni_{0.4}Mn_{0.4}Co_{0.2}]O_2$ (NMC442), $Li[Ni_{0.5}Mn_{0.3}Co_{0.2}]O_2$ (NMC532), $Li[Ni_{0.6}Mn_{0.2}Co_{0.2}]O_2$, and $Li[Ni_{0.2}Mn_{0.2}Co_{0.6}]O_2$. As expected, these known single-phase samples fall within or very near the boundaries of the single-phase regions determined here. If NMC442 and NMC532 are synthesized with a slight lithium excess, for regular cooled samples, they move into the single phase region. Evidence for the various features observed in the

DOI: 10.1021/acscombsci.5b00048
ACS Comb. Sci. 2015, 17, 381−391

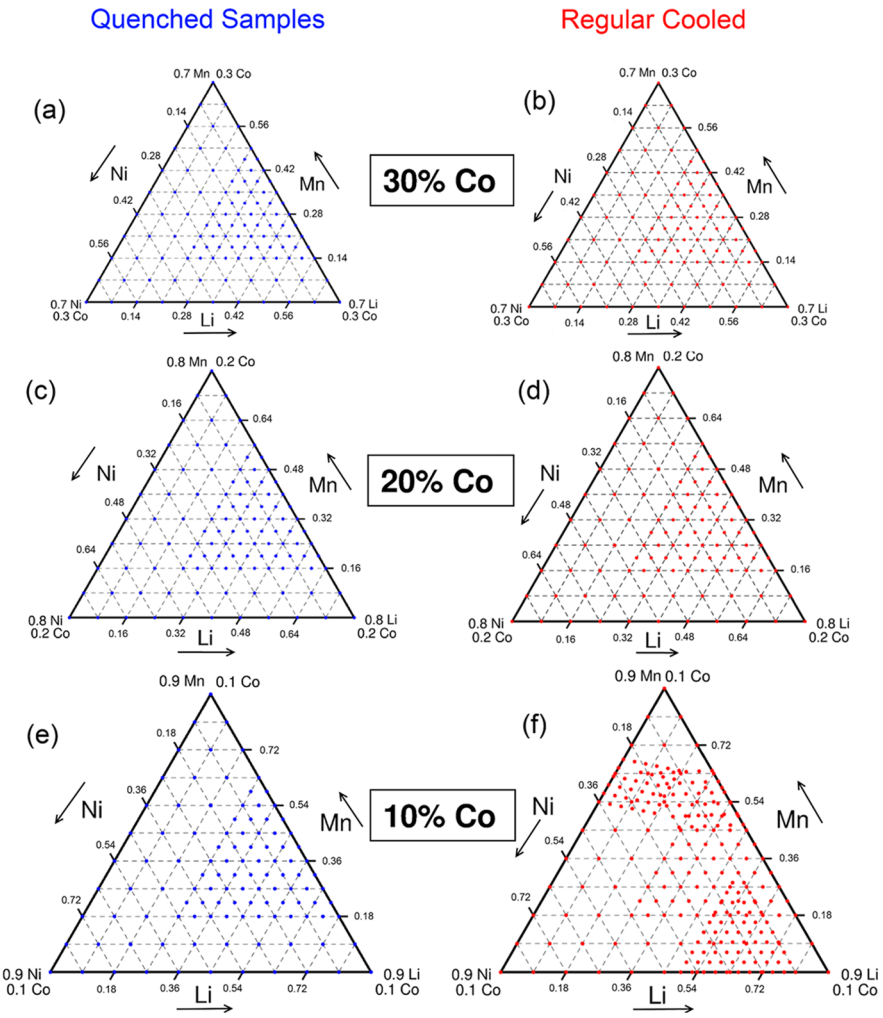

Figure 2. Plots showing the compositions synthesized to map out the 10%, 20%, and 30% cobalt slice ternary phase diagrams within the Li−Ni−Mn−Co−O pseudoquaternary system. Quenched samples are indicated by blue dots in panels a, c, and e, and regular-cooled samples are indicated by red dots in panels b, d, and f. All samples were heated to 800 °C for 3 h in oxygen before being cooled by the indicated cooling rate. The axes are labeled by their respective elements and range of fractional content. The cobalt content in each pair of cobalt slices are as follows: (a, b) 30% cobalt content, (c, d) 20% cobalt content, and (e, f) 10% cobalt content.

series of cobalt slice phase diagrams of Figures 3 and 4 will be presented here.

Elemental Analysis. Figure 5 shows ICP-OES elemental analysis results for samples located near the Li-rich corner ($Li_{0.9}Co_{0.1}$) of the regular-cooled 10% cobalt slice ternary phase diagram. The blue and green arrows in Figure 5 point from the initial compositions targeted during dispensing to the compositions measured after synthesis by ICP elemental analysis. These arrows tended to radiate away from the Li-rich corner and their magnitudes decrease with lower initial lithium content. These observations support previous results that concluded lithium loss due to the formation of Li_2O_2 is a major factor to consider when synthesizing combinatorial samples in the lithium-rich region of the Li−Ni−Mn−Co−O system.[4,14] The removal of lithium from a sample forces its composition away from the lithium corner of the pseudoquaternary system (e.g., a sample initially dispensed at $Li_{0.70}Ni_{0.10}Mn_{0.10}Co_{0.10}$ that experiences 9% lithium loss will have a resulting composition of $Li_{0.61}Ni_{0.13}Mn_{0.13}Co_{0.13}$). As a result, the final compositions of samples shown in Figure 5 actually have cobalt fractional metal contents higher than 10% as plotted. The highest measured cobalt fractional metal content in Figure 5 was Co = 0.151 ± 0.008 for the sample dispensed at (Ni = 0.081, Mn = 0.036, Co = 0.100) and the average measured cobalt fractional metal content for samples dispensed inside or above the single-phase layered region was Co = 0.104 ± 0.001. In order to plot all compositions on the same ternary diagram, the measured compositions had their cobalt contents set to 10% of the total composition and the remaining 90% of the composition was composed of Li, Ni, and Mn in the same ratio as was measured. As a result, the measured compositions are located at the same relative positions in the cobalt slice of Figure 5 as in their respective real cobalt slice ternary phase diagrams.

Since samples at higher initial lithium contents experience more lithium loss during heating, samples dispensed at lower initial lithium contents than those shown in Figure 5 are expected to experience less amounts of lithium loss and, as a result, have more accurate final compositions.[4,14] Furthermore, as cobalt content increases lithium loss diminishes, even for small combinatorial samples.[14] Thus, the compositions shown in Figure 5 are the worse-case scenarios for lithium loss in this system, but even here the loss is manageable within the single phase region (i.e., between the two red lines the arrows typically result in a lithium loss of no more than 5%). On the basis of this

DOI: 10.1021/acscombsci.5b00048
ACS Comb. Sci. 2015, 17, 381−391

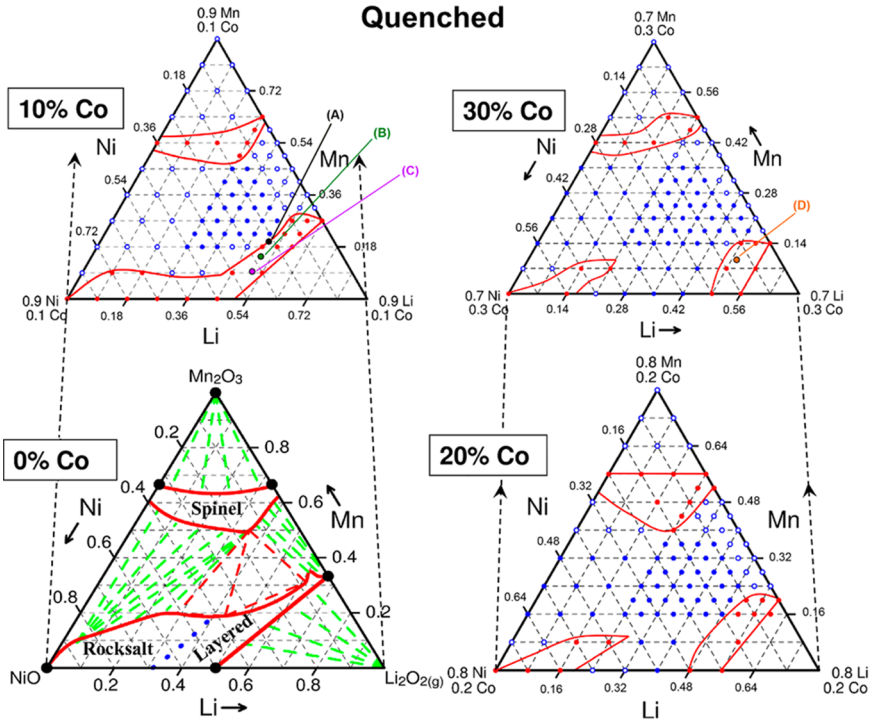

Figure 3. Stack of cobalt slice ternary phase diagrams in the Li−Ni−Mn−Co−O pseudoquaternary system at cobalt contents of 0%, 10%, 20%, and 30% for samples quenched after heating to 800 °C for 3 h in oxygen. The included Li−Ni−Mn−O pseudoternary phase diagram for quenched samples was determined by McCalla et al. and reprinted with permission from the American Chemical Society.[5] Red dots indicate compositions determined to be single-phase, open blue dots indicate samples containing two phases and filled blue dots indicate samples containing at least three distinct phases. Solid red lines define boundaries to single-phase regions as determined by dividing regions containing single-phase compositions with those containing multiphase. Common industrial compositions are labeled on the phase diagrams as follows: (A) $Li[Ni_{0.4}Mn_{0.4}Co_{0.2}]O_2$ in black, (B) $Li[Ni_{0.5}Mn_{0.3}Co_{0.2}]O_2$ in green, (C) $Li[Ni_{0.6}Mn_{0.2}Co_{0.2}]O_2$ in purple, and (D) $Li[Ni_{0.2}Mn_{0.2}Co_{0.6}]O_2$ in orange. The same conventions are followed in Figure 4

figure and the 3% uncertainty on the concentrations of the starting materials, we estimate that the final compositions are within 5% of their dispensed compositions for all samples lying in the single-phase layered region or with less lithium than the layered materials, with this number decreasing as the cobalt content increases, and also as the lithium content decreases.

The effect of random experimental error on compositional accuracy can also be observed in Figure 5 by the direction of the arrows. If lithium loss were the only effect creating the observed differences in composition, the arrows in Figure 5 would be expected to diverge from the Li-rich corner. Although the majority of arrows in Figure 5 follow this ideal pattern fairly well, there are some that point in directions that indicate non-stoichiometries not explained by the loss of lithium (e.g., the arrow representing the sample dispensed with the metal content $Li_{0.525}Ni_{0.185}Mn_{0.190}Co_{0.100}$ points away from the Ni corner, indicating a lower fractional nickel content in the final composition). As there are no mechanisms for such an effect to occur, this result is attributed to the uncertainty in the concentrations of the dispensing solutions.

Figure 6 shows the fitted XRD patterns for the samples showing the greatest lithium loss, represented by green arrows in Figure 5. All XRD patterns shown in Figure 6 were fit as single-phase layered structures and the quality of the resulting fits indicate that the samples have single-phase hexagonal layered structures. This result, in combination with the observations of Figure 5, confirm that the compositions of samples dispensed between the single-phase layered region and the Li-rich corner shift due to lithium loss such that the resulting compositions are within the single-phase layered region. The corresponding green arrows for these samples in Figure 5 do not extend to the single-phase layered region as drawn, however these samples were measured to have cobalt fractional metal contents ranging from 0.130 ± 0.007 to 0.151 ± 0.008, which means their final compositions each exist on specific ternary planes between the 10% and 20% cobalt slice phase diagrams shown in Figure 4. As it will be demonstrated in the following section, the addition of cobalt forces the single-phase layered region to approach closer to the Li−Co edge of the quaternary diagram and it in fact extends entirely to the Li−Co edge for the 50% cobalt slice because $LiCoO_2$ exists on this plane.

Layered and Rocksalt Single-Phase Regions. Figure 3 shows the 10%, 20%, and 30% cobalt slice ternary phase diagrams for samples heated to 800 °C under oxygen flow before being quenched to room temperature. Figure 4 shows an identical series of cobalt slice phase diagrams obtained for regular-cooled samples. As was true for the Li−Ni−Mn−O pseudoternary system, a large single-phase layered-rocksalt region was found to exist at compositions with low Mn content within the 10% cobalt slice ternary systems for both quenched and regular-cooled samples. In the 20% and 30% cobalt slice ternary systems for both cooling rates, the single-phase layered-rocksalt region phase separated into distinct cubic rocksalt and hexagonal layered single-phase regions with a coexistence region existing between them.

Figure 7 shows XRD patterns for compositions extending across the lithium-rich portion of the single-phase layered region of the regular-cooled 10% cobalt slice ternary phase diagram. The

DOI: 10.1021/acscombsci.5b00048
ACS Comb. Sci. 2015, 17, 381−391

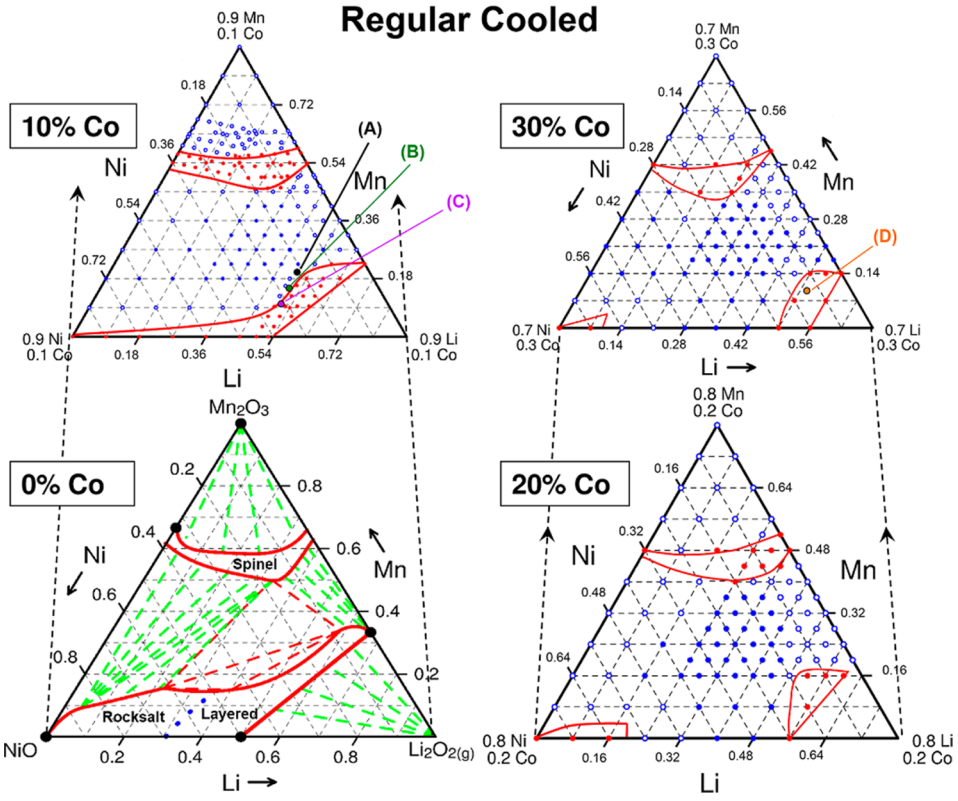

Figure 4. Stack of cobalt slice ternary phase diagrams in the Li−Ni−Mn−Co−O pseudoquaternary system at cobalt contents of 0%, 10%, 20%, and 30% for samples regular-cooled after heating to 800 °C for 3 h in oxygen. The included Li−Ni−Mn−O pseudoternary phase diagram for regular-cooled samples was determined by McCalla et al. and reprinted with permission from the American Chemical Society.[5]

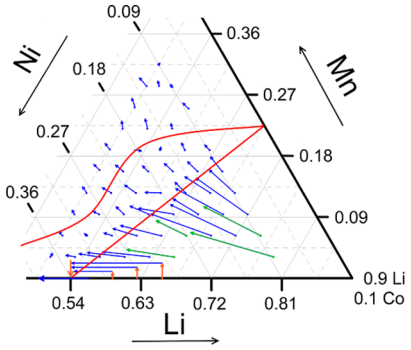

Figure 5. Plot of the elemental analysis results for samples with compositions located near the Li−Co edge of the 10% cobalt slice ternary phase diagram within the Li−Ni−Mn−Co−O system. The samples shown were all heated to 800 °C in oxygen before undergoing regular-cooling. The blue and green arrows point away from the targeted compositions to the final compositions of samples after synthesis as measured by ICP elemental analysis. Samples represented by green arrows are referenced in the text. The orange arrows help distinguish the composition shifts occurring along the bottom axis. The red lines define the boundaries to the single-phase layered region as determined by the current study.

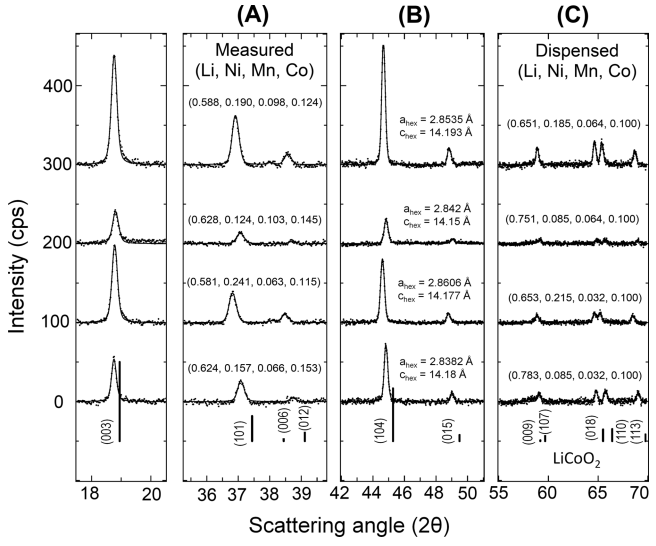

Figure 6. Stack of fitted XRD patterns for compositions dispensed near the Li−Co edge of the 10% cobalt slice ternary phase diagram (green arrows in Figure 5). Measured compositions of each sample are provided in column (A) and initial compositions are labeled in column (C). Fitted lattice parameters are reported in column (B). The XRD patterns are plotted as black dots and the resulting fits are drawn as solid lines. The vertical lines represent the database spectra for $LiCoO_2$ (JCPDS 77-1370) and each peak is labeled with its corresponding (*hkl*) indices.

gradual shift in diffraction peak positions to higher angles between the XRD patterns of samples A−G in Figure 7 indicates the existence of a solid solution extending across the corresponding composition region. Table S.1 (Supporting Information) shows values for all hexagonal lattice parameters obtained for single-phase layered samples in this study. Of particular interest, the samples corresponding to the end point XRD patterns of samples A and G in Figure 7 have structures resembling $LiNiO_2$ (JCPDS 89-3601) and Li_2MnO_3 (JCPDS 84-1634), respectively, with minor peak shifts to higher angles because of smaller lattice parameters. The XRD pattern of

DOI: 10.1021/acscombsci.5b00048
ACS Comb. Sci. 2015, 17, 381−391

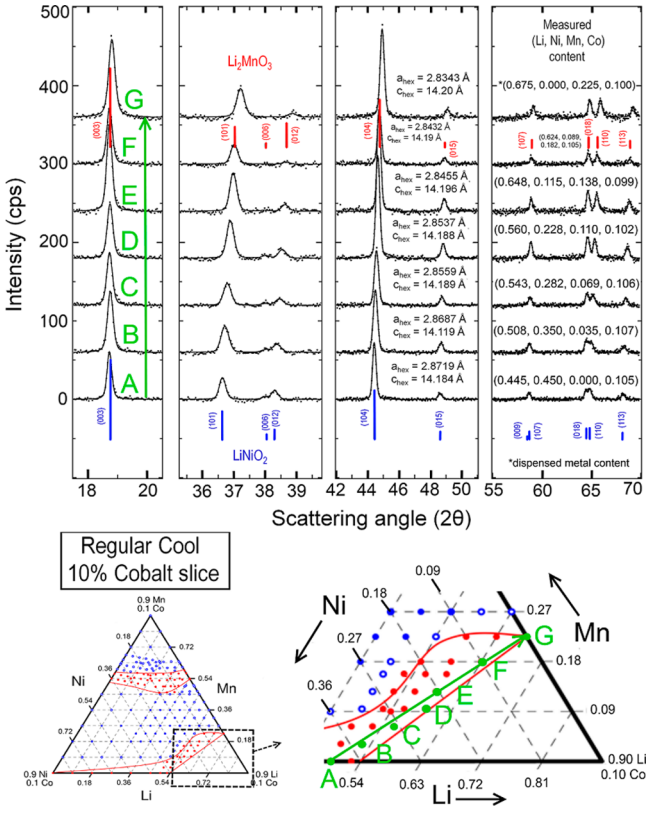

Figure 7. Fitted XRD patterns for samples of the regular-cooled 10% cobalt slice ternary system indicating the existence of a solid solution through the determined single-phase layered region. Every second data point within the XRD patterns are plotted in order to improve their clarity. Blue and red vertical lines represent the database spectra for $LiNiO_2$ (JCPDS 89-3601) and Li_2MnO_3 (JCPDS 84-1634), respectively, and corresponding (*hkl*) indices for each peak are labeled. Samples A–G and have positions indicated on the included phase diagram. Measured fractional metal contents are provided, except for sample G, which was not measured and instead has its dispensed composition reported. Fitted lattice parameters are reported in the third column.

sample A in Figure 7, corresponding to a sample with measured fractional metal contents of $Li_{0.445}Ni_{0.450}Co_{0.105}$, had fitted lattice parameters of a_{hex} = 2.8719 ± 0.0007 Å and c_{hex} = 14.194 ± 0.008 Å, which compared well with database values of a_{hex} = 2.8762 Å and c_{hex} =14.190 Å for the nearby composition $LiNiO_2$. Sample G in Figure 7 did not have its final composition measured and was thus referred to by its dispensed fractional metal contents of $Li_{0.625}Mn_{0.225}Co_{0.100}$. This sample had fitted lattice parameters of a_{hex} = 2.8343 ± 0.0004 Å and c_{hex} = 14.20 ± 0.01 Å, which were slightly lower than the database values of a_{hex} = 2.845 Å and c_{hex} = 14.2004 Å for the nearby composition Li_2MnO_3.

The lower lattice parameters of samples A and G when compared to the database structures included in Figure 7 are the result of increasing cobalt content. Previous work in the Li–Co–Mn–O pseudoternary phase diagram shows that the layered structure with the highest cobalt content is $LiCoO_2$, which has significantly smaller lattice parameters than each of A and G: a_{hex} = 2.815 Å and c_{hex} = 14.05 Å.[13] Thus, as cobalt content increases, a corresponding decrease in both lattice parameters is expected.

It is important to note the minor amount of peak broadening occurring in the XRD pattern of sample G in Figure 7 that could be indicative of layered–layered phase separation beginning to occur. Previous results on the layered solid solution line in the Li–Co–Mn–O pseudoternary system determined that samples prepared there with Co fractional metal contents ranging from 0.12 to 0.28 phase separate to layered–layered two-phase materials when regular-cooled.[4,15] As the composition of sample G was not measured, the final cobalt content can only be extrapolated from the elemental analysis results of the previous section, which observed an average cobalt content of Co = 0.104 ± 0.001 for regular-cooled samples dispensed within the single-phase layered region. This sample lies therefore at the edge of where phase separation is expected to occur, so the small amount of broadening may be due to the onset of phase separation.

Figure 8 shows three stacks of XRD patterns corresponding to samples synthesized along the non-Mn-containing axis of each

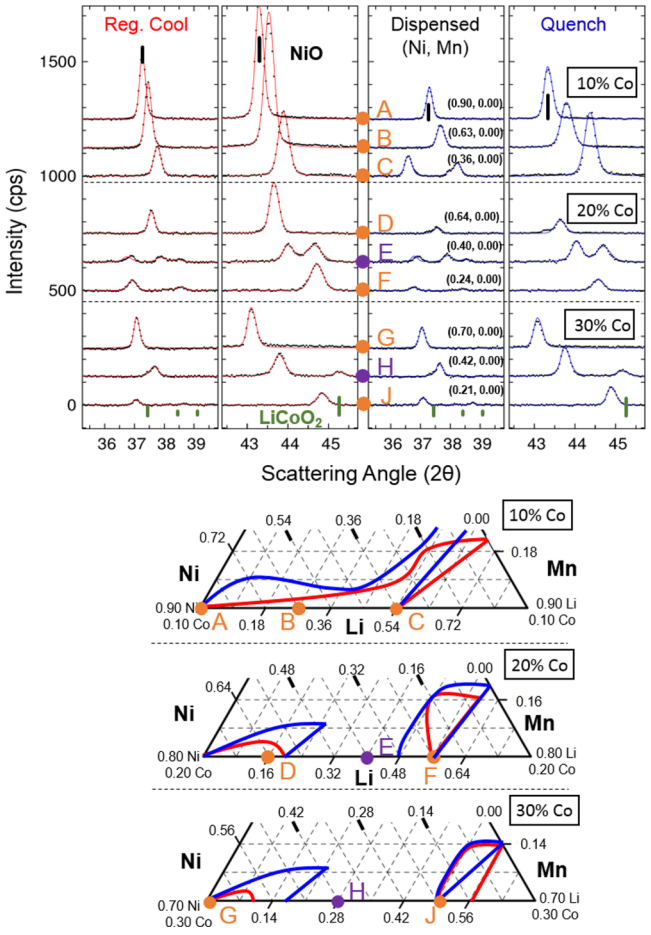

Figure 8. Stacks of fitted XRD patterns for samples synthesized along the non-Mn-containing axis of each cobalt slice ternary phase diagram. Regular-cooled XRD patterns and single-phase boundary lines are drawn in red and quenched in blue. Dispensed (Ni, Mn) contents of samples are provided and corresponding locations on the phase diagram are indicated by orange and purple dots for single-phase and multiphase, respectively. All fitted peaks were indexed by the $R\bar{3}m$ space group for hexagonal structures and multiphase fits had two sets of peaks indexed. The black and green vertical lines correspond to the database spectra for NiO (JCPDS 44-1159) and $LiCoO_2$ (JCPDS 77-1370).

cobalt slice ternary phase diagram (i.e., the portions of cobalt slices existing on the Li–Ni–Co face of the pseudoquaternary system as shown in Figure 1). The relevant regions of the cobalt slice ternary phase diagrams are included in Figure 8 with the single-phase boundaries drawn for both cooling rates as determined by visually determining whether the XRD patterns

DOI: 10.1021/acscombsci.5b00048
ACS Comb. Sci. 2015, 17, 381–391

are single-phase or multiphase. The cubic rocksalt single-phase region was observed to be smaller for regular-cooled samples than for quenched samples. The reasoning for the observed shift resulting from cooling rate is likely related to the differences in oxygen content between quenched and regular-cooled samples. Phases of higher oxygen content, such as spinel Mn_3O_4, form more easily for materials with higher available oxygen content, as compared to layered structures of the form M_2O_2 that have a lower oxygen content. Since combinatorial samples lose significant amounts of oxygen during heating due to the high surface-area-to-volume ratio, they will be oxygen deficient unless cooled slowly to allow for oxygen reuptake (i.e., regular cooling) and favor the formation of lower oxygen content structures. These considerations help explain the observations for the single-phase cubic rocksalt regions existing over a larger composition range for quenched samples than for regular-cooled samples within every cobalt slice shown in Figure 8.

The hexagonal layered single-phase region showed similar size differences between quenched and regular-cooled samples in the 10%, 20%, and 30% cobalt slice ternary systems. As is shown in Figure 8, the hexagonal layered region of the regular-cooled 20% cobalt slice ternary system did not fully extend to the Li−Co−Mn face of the pseudoquaternary phase system. The regular-cooled sample dispensed at the composition $Li_{0.60}Mn_{0.20}Co_{0.20}$ on the non-Ni-containing axis of the 20% cobalt slice was determined to be a layered−layered phase separated material by XRD analysis (not shown here). This observation agrees with previous results indicating layered−layered phase separation occurring in regular-cooled layered materials of the Li−Co−Mn−O pseudoternary system with Co fractional metal contents ranging from 0.12 to 0.28.[4,15]

Although the samples corresponding to XRD patterns plotted in Figure 8 are labeled by their dispensed fractional metal contents and not measured contents, the effects of lithium loss on the XRD patterns can be observed by comparing the data between the two cooling rates. A dramatic example of this is observed in the pair of XRD scans corresponding to a quenched and a regular-cooled sample dispensed with fractional metal contents of $Li_{0.45}Ni_{0.45}Co_{0.10}$ (label C in Figure 8). The structure of the quenched sample at this composition was determined to be a single-phase hexagonal layered, while the corresponding regular-cooled sample had its structure determined to be single-phase cubic rocksalt due to having a c/a ratio of 4.91 ± 0.02, which is within error of the value $\sqrt{24}$, which is the value expected for cubic rocksalt structures.[16] The different phases observed in samples of composition 'C' of Figure 8 between cooling rates implies either that the regular-cooled sample contained a higher nickel fractional metal content following synthesis than the quenched sample that allowed for the formation of a rocksalt phase during cooling, or that the rocksalt phase is simply preferred at this composition for samples cooled more slowly. Although more lithium loss is expected for regular-cooled samples since they spend more time at elevated temperatures, this has typically proven to be small in our combinatorial studies.[4,14] Thus, this strange behavior warrants further study in the Li−Co−Ni−O system, as movement of the rocksalt-layered phase transition within the Li−Ni−Mn−O system was never seen.[4]

Samples made at compositions E and H labeled in Figure 8 had their XRD patterns calculated with two sets of diffraction peaks indexed by the $R\bar{3}m$ space group for hexagonal layered structures. The resulting fitted XRD patterns determined that these compositions phase separated into distinct layered and rocksalt phases, and sample E had an additional third phase that was not identified. The unfitted data seen within the XRD patterns of the regular-cooled and quenched samples of composition E in Figure 8 are indicative of the unfitted third phase present in these samples. It is difficult to conclude the identity of the third phase without performing a three-phase fit, which was not performed for the current work. Interestingly, the fitted multiphase XRD patterns shown in Figure 8 had little variation between quenched and regular-cooled samples of the same composition, which is contrasted by the significant differences observed between the XRD patterns of quenched and regular-cooled single-phase samples. This suggests that these multiphase compositions are composed of very similar phases regardless of cooling rate. As there was no Mn present in any of the samples shown in Figure 8, these samples exist on the Li−Ni−Co face of the pseudoquaternary system. Therefore, there must exist a three-phase region within the Li−Ni−Co−O pseudoternary system. Further study of this system is warranted to clearly establish the nature of these coexistence regions.

Single-Phase Cubic Spinel Region. Figure 9 shows stacks of XRD patterns corresponding to samples A−I of compositions

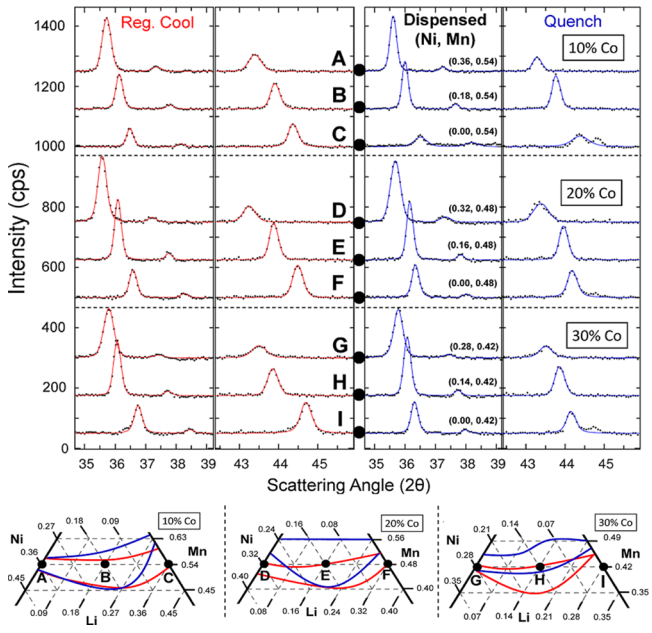

Figure 9. Stacks of fitted XRD patterns for samples synthesized at constant manganese content through the single-phase cubic spinel region of each cobalt slice ternary phase diagram. Regular-cooled XRD patterns and single-phase boundary lines are drawn in red and quenched in blue. Dispensed (Ni, Mn) contents of samples are provided and their corresponding locations on the phase diagram are highlighted by the labels A−I. All fitted peaks were indexed by the $Fd\bar{3}m$ space group for cubic structures.

with constant manganese content across the single-phase cubic spinel region of the 10%, 20%, and 30% cobalt slice ternary phase diagrams. The relevant regions of the corresponding phase diagrams are included in Figure 9 with the single-phase boundaries drawn for both cooling rates as determined by visually distinguishing single-phase patterns from multiphase. The fitted XRD patterns in Figure 9 were determined by having diffraction peaks indexed in the $Fd\bar{3}m$ space group for cubic structures. Multiphase samples in Figure 9 were identified by the presence of unfitted diffraction peaks in the XRD patterns. A

DOI: 10.1021/acscombsci.5b00048
ACS Comb. Sci. 2015, 17, 381−391

separate two-phase fitting was performed on such samples to confirm the identity of the extra phase. For example, the XRD pattern labeled F in Figure 9 corresponding to the quenched sample of dispensed fractional metal contents $Li_{0.12}Ni_{0.00}Mn_{0.48}Co_{0.20}$ had an unfitted peak near $2\theta = 48°$, which was determined to be the (104) peak of a hexagonal layered phase and was subsequently fit using a two-phase fitting routine.

It is important to note that Figure 9 is not a complete survey of all the single-phase compositions found to exist within the single-phase cubic spinel regions of the cobalt slice ternary phase diagrams. The intended purpose of Figure 9 is to demonstrate how the single-phase cubic spinel boundaries presented in Figures 3 and 4 were determined and also to demonstrate the effect of cooling rate on the position of the single-phase boundaries. All single-phase compositions used to determine the boundaries of the single-phase regions in the cobalt slice ternary systems, along with their corresponding fitted lattice parameters, have been cataloged in Table S.2 (Supporting Information).

The portions of the cobalt slice ternary phase diagrams included in Figure 9 show the single-phase spinel regions for both quenched and regular-cooled samples. The upper and lower boundaries of the regular-cooled single-phase spinel regions were found to exist at compositions of lower Mn content compared to the corresponding quenched regions. This result is consistent with observations in the Li−Co−Mn−O pseudoternary system and also the Li−Ni−Mn−O pseudoternary system.[4,5,13] The difference in oxygen content between quenched and regular-cooled samples is again the likely culprit for the observed differences in phase region boundaries as explained before in the single-phase layered region. In the case for the single-phase spinel region, the bixbyite Mn_2O_3 structure is able to form more easily in materials with higher available oxygen content, which causes the single-phase spinel region (characterized by M_3O_4 structures) to be smaller for regular-cooled samples when compared to the quenched system. Furthermore, the coexistence region above the single-phase spinel region is enlarged for regular-cooled samples, which can be observed by comparing the quenched cobalt slices of Figure 3 with corresponding regular-cooled cobalt slices in Figure 4. The diffraction peaks of samples shown in Figure 9 all shifted to lower values of 2θ when replacing Li with Ni in their compositions (i.e., samples from right to left across each phase diagram in Figure 9). The observed peak shifts corresponded to an increase in lattice parameter due to the replacement of Li atoms by Ni atoms at octahedral sites within the spinel structure. In the regular-cooled 10% cobalt slice ternary system, the observed spinel solid solution extending from the fractional metal contents of $Li_{0.36}Mn_{0.54}Co_{0.10}$ (composition C in Figure 9) to $Ni_{0.36}Mn_{0.54}Co_{0.10}$ (composition A in Figure 9) had measured lattice parameters of $a_{cub} = 8.153 \pm 0.002$ and 8.354 ± 0.002 Å, respectively, at these end point compositions. For the corresponding quenched samples, the lattice parameters of the spinel phase were measured to be $a_{cub} = 8.164 \pm 0.007$ and 8.356 ± 0.002 Å, respectively. However, it should be noted that the quenched sample of composition C in Figure 9 was not single-phase as determined by the unfitted peak near $2\theta = 48°$ its XRD pattern that corresponds to the (104) peak of a hexagonal layered phase. Thus, the general trend that lattice parameters decrease as lithium content increases is followed here.

At 20% and 30% cobalt fractional metal content, the lattice parameters of the spinel phase in the compositions of Figure 9 tend to decrease until reaching a minimum value of $a_{cub} = 8.099 \pm 0.002$ Å for the regular-cooled sample of composition I dispensed at fraction metal content $Li_{0.08}Mn_{0.42}Co_{0.30}$. This composition exists within the spinel-layered coexistence region of the Li−Co−Mn−O pseudoternary system and is expected to tie to a cobalt-rich spinel phase in the vicinity of the cobalt corner. The Co_3O_4 spinel phase is the end point cobalt composition within the single-phase spinel region of the Li−Ni−Mn−Co−O pseudoquaternary system and it has a lattice parameter of $a_{cub} = 8.084 \pm 0.004$ Å as reported in ref 13. Since the lattice parameter of the spinel phase in the regular-cooled sample of composition I was close to the value of Co_3O_4, it matches the results predicted by the phase diagrams of previous work.[13]

It is expected that increasing the cobalt content of cubic spinel materials will decrease their lattice parameter, given that Co_3O_4 has such a small lattice parameter. The fitted lattice parameters reported in Figure 9 follow this pattern, as the lowest lattice parameters were measured for samples dispensed at the highest Co metal fraction of 0.30. This result suggests that the cobalt content of a spinel phase in a multiphase sample within the Li−Ni−Mn−Co−O pseudoternary system could potentially be characterized by its lattice parameter (e.g., a lower cubic lattice parameter means higher cobalt content and vice versa). A full survey of the pseudoquaternary system would be required to accurately determine the structure of tie-lines and describe how the single-phase spinel and layered regions connect through their coexistence regions. However, this may still prove difficult as the multiphase samples can now tie to any point on a 2-D surface making it very difficult to determine the tie-line end-members using a single lattice parameter.

Figure 10 shows contour plots of the fitted lattice parameters for compositions within the single-phase layered region of the regular-cooled 10% cobalt slice ternary system, in addition to a contour plot of unit cell volume per O_2 unit for both the cubic spinel and hexagonal layered regions of the same system. Calculating the volume per O_2 unit in each structure allows for the direct comparison of the lattice parameters between the layered and cubic spinel structures. The contour plots of O_2 unit volume were determined by dividing calculated cubic spinel unit cell volumes by 16 and layered unit cell volumes by 3. The divisor values were determined from theoretical crystal structure considerations of the cubic spinel and layered structures whereby 32 oxygen atoms exist in the unit cell of a cubic spinel structure M_3O_4 and 6 oxygen atoms exist in the unit cell of a layered structure M_2O_2. Therefore, there is a 16:3 ratio between the number of oxygen atoms in the spinel and layered unit cells.

The major observation that can be seen in Figure 10c is that increasing Li content decreases the volume per O_2 unit. Both the spinel and layered regions of Figure 10c experienced a decrease in O_2 unit volume as Li replaced either Ni or Mn within either structure. Furthermore, it appeared that there was little effect on the volume from replacing Ni with Mn or vice versa, as indicated by the tendency of the contour lines in Figure 10 to run parallel with grid lines of constant Li content. Since the layered contour plots in Figure 10a−c had no single-phase samples dispensed above the Li−Ni−Co edge from Li = 0.00 to 0.50, the contour lines in Figure 10 along the non-Mn-containing edge are only accurate near this face of the pyramid, as drawn. These contour lines should not be extrapolated to areas where no samples were prepared.

The location of the phase transition between the rocksalt and layered phases was not determined for either the quenched or regular-cooled 10% cobalt slice ternary. However, the existence of such a phase transition is highly likely as there were no rocksalt-layered multiphase samples observed along the non-Mn-

DOI: 10.1021/acscombsci.5b00048
ACS Comb. Sci. 2015, 17, 381−391

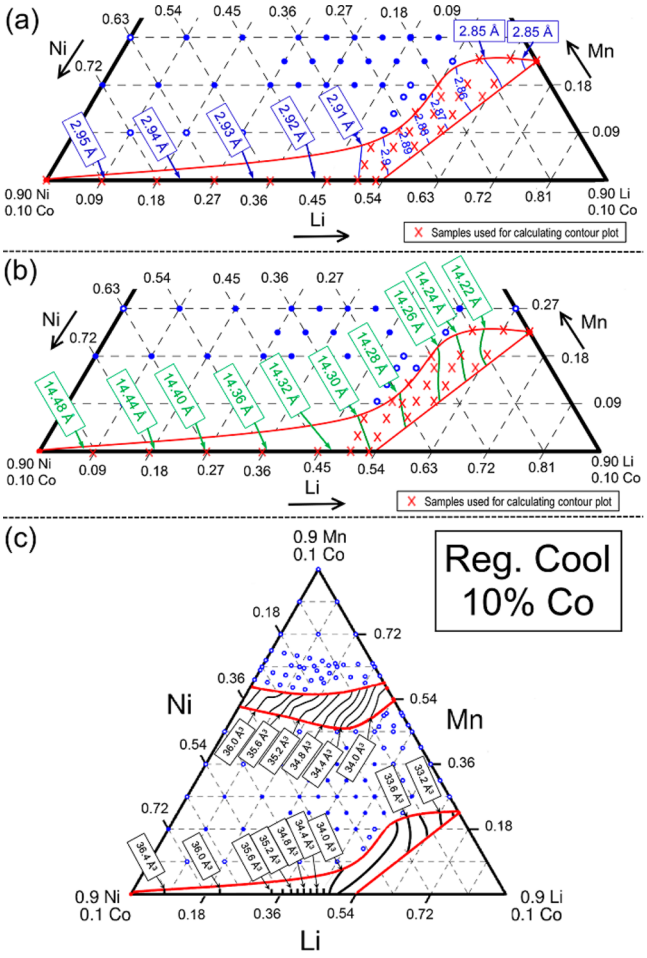

Figure 10. Contour plots of the (a) fitted a_{hex} lattice parameters, (b) fitted c_{hex} lattice parameters of the single-phase layered region in the regular-cooled 10% cobalt slice ternary phase diagram, and (c) contour plots of unit cell volume per MO_2 basis unit for both the cubic spinel and layered single-phase regions within the regular-cooled 10% cobalt slice. In panel c, unit cell volumes were calculated from fitted lattice parameters and then scaled by the number of metal atoms in octahedral sites for each structure. The divisor was 16 for cubic spinel (M_3O_4 in $Fd\bar{3}m$ space group) and 3 for the hexagonal layered ($LiMO_2$ in $R\bar{3}m$ space group).

containing edge of this cobalt slice. Since the structures must change from one to the other at some composition, there must be either a phase transition line or a small coexistence region existing between the compositions observed. A higher sampling density in this region would be required in order to make a definitive conclusion regarding the phase separation between the rocksalt and layered phases in the quenched or regular-cooled 10% cobalt slice ternary.

Layered-Spinel Coexistence Regions. It would be useful to also understand the coexistence regions existing between the spinel and layered single-phase regions of the Li−Ni−Mn−Co−O pseudoquaternary system for research on composite positive electrode materials. The task of determining the tie-lines as well as end points of any 3- or 4-phase regions is beyond the scope of the current work. The spinel-layered coexistence regions of the Li−Ni−Mn−Co−O pseudoternary system are characterized by the multiphase samples represented by the empty and filled blue circles located between the spinel and layered regions of each cobalt slice ternary in Figures 3 and 4. The multiphase samples in this work were each fit by a two-phase fitting routine with peaks indexed by either a combination of one cubic spinel and one hexagonal layered structure, or two hexagonal layered structures. Many of the multiphase samples found in these regions contained more than two phases as indicated by unfitted peaks remaining in the fitted XRD patterns. Results from this project were found to corroborate previous observations in the coexistence regions of the Li−Ni−Mn−O pseudoternary system.[4,5] Specifically, there was evidence found to support the existence of separate spinel-layered and spinel-rocksalt coexistence regions within the quenched 20% cobalt slice of the Li−Ni−Mn−Co−O pseudoquaternary system, as well as regions with at least three phases in the 10% cobalt slice.

Figure 11 shows XRD patterns corresponding to quenched samples in the 20% cobalt slice ternary system with compositions highlighted on the included phase diagram. The XRD pattern labeled 2 was fit as single-phase cubic spinel, while the patterns labeled 1 and 3 were fit as a combination of cubic spinel and hexagonal layered structures. The c/a ratio of the hexagonal layered fitted parameters of sample 3 was calculated to be 4.90 ± 0.01, which is within error to the value of $\sqrt{24}$ expected for parameters corresponding to a cubic rocksalt structure.[16] The fitted XRD pattern of sample 1 in Figure 11 was found to contain a hexagonal layered phase in combination with a cubic spinel phase. These results suggest that there are at least two separate coexistence regions existing within the multiphase region of the Li−Ni−Mn−Co−O pseudoquaternary system: a spinel-rocksalt coexistence region and a spinel-layered coexistence region. This result is similar to those found in the coexistence regions of the Li−Ni−Mn−O pseudoternary system wherein tie-lines were defined for various rocksalt-spinel and layered-spinel multiphase materials.[4,5] However, determining the tie-lines for multiphase materials within the cobalt slices is a far more difficult task due to the possibility that the constituent phases making up the multiphase samples may have different cobalt contents such that tie-lines do not necessarily lie in plane with the ternary diagrams drawn throughout this paper.

The cubic spinel phase of the multiphase samples in Figure 11 were found to have lattice parameters of a_{cub} = 8.194 ± 0.002 and 8.237 ± 0.002 Å for compositions labeled 1 and 3, respectively, while the single-phase composition labeled 2 had a lattice parameter of a_{cub} = 8.206 ± 0.002 Å. The results of the previous section showed that the lattice parameter of single-phase spinel materials increased with nickel content, but also decreased with increased cobalt content. This makes it impossible to determine the compositions of the spinel phases in samples 1 and 3 from a single lattice parameter, since there must be a lattice parameter contour line along the surface of the spinel region where Ni is substituted for Co. This illustrates the immense challenge in determining the coexistence regions within a quaternary system. Nonetheless, the determination of the boundaries of the single-phase regions will be of significant value to the lithium-ion battery community.

CONCLUSIONS

The cubic spinel and layered-rocksalt single-phase regions of the 10%, 20%, and 30% cobalt slice ternaries of the Li−Ni−Mn−Co−O pseudoquaternary system were determined for quenched and regular-cooled samples. The fitted lattice parameters of the single-phase materials observed in these systems have been cataloged in the Supporting Information section for referencing purposes. The effects of lithium loss during heating were studied through a series of ICP elemental analysis measurements on samples synthesized within the lithium-rich region of the regular-

DOI: 10.1021/acscombsci.5b00048
ACS Comb. Sci. 2015, 17, 381−391

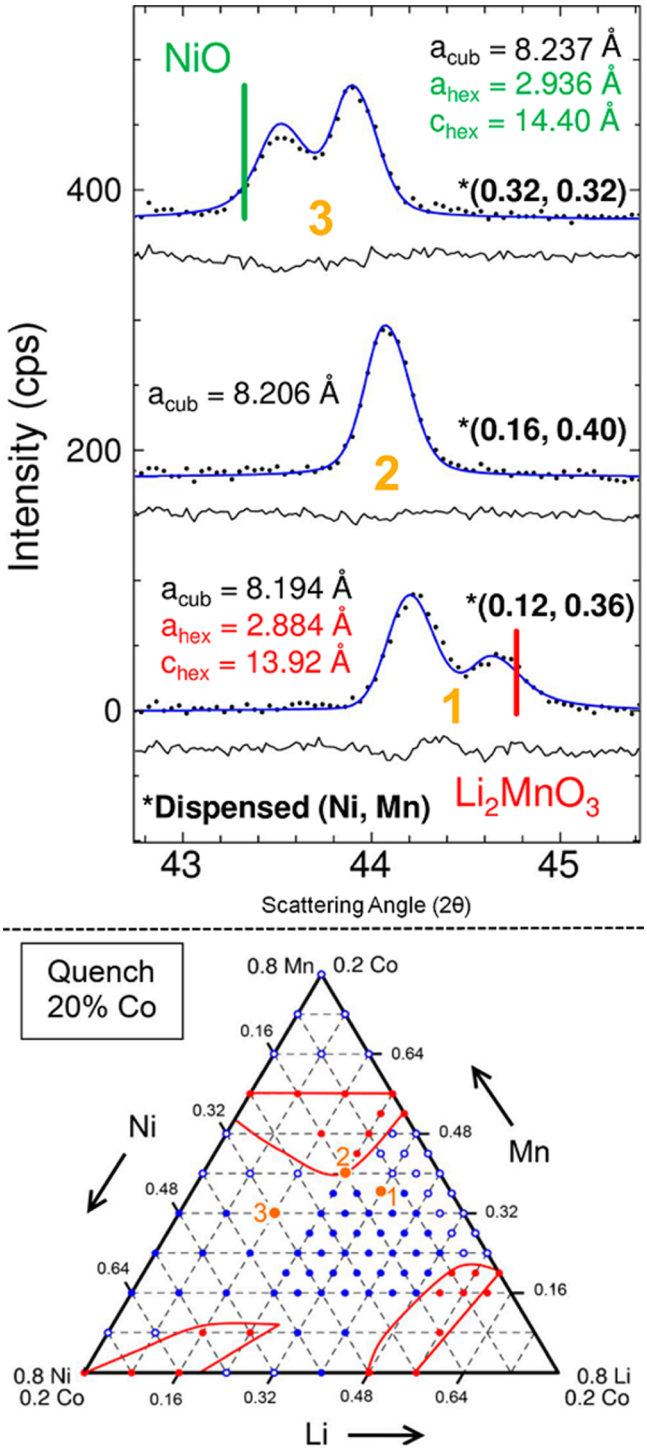

Figure 11. XRD patterns corresponding to quenched samples of compositions near the lower boundary to the single-phase spinel region in the 20% cobalt slice. Dispensed (Ni, Mn) fractional metal contents of each sample are given and corresponding locations are highlighted in orange on the phase diagram. Samples 1 and 3 had XRD patterns fit using two sets of peaks indexed by cubic spinel and hexagonal layered structures, while the XRD pattern of sample 2 was fit using peaks only indexed as cubic spinel. Green and red vertical lines represent the database (104) peak of NiO (JCPDS 44-1159) and Li_2MnO_3 (JCPDS 84-1634) respectively. Difference plots are shown in black line under each fit.

cooled 10% cobalt slice ternary. Samples dispensed within the single-phase layered region experienced an average lithium loss of roughly 1−5%. Lithium loss was found to be most severe in samples dispensed in the region between the single-phase layered region and the Li−Co edge of the pseudoquaternary system. The lithium loss experienced by such samples caused their final composition to lie within the single-phase layered region.

The rocksalt-layered single-phase region of the pseudoquaternary system was found to phase separate for higher cobalt content (i.e., for both the 20% and 30% slices) for both quenched and regular-cooled samples. The addition of 10% cobalt content to the Li−Ni−Mn−O pseudoternary system caused the layered-rocksalt single-phase region to decrease in size for samples of both cooling rates studied, but otherwise the phase diagram looked very similar. For the composition regions investigated, the single-phase layered and rocksalt regions remained significantly larger for quenched samples than for regular-cooled samples. At 20% cobalt content, the hexagonal layered single-phase region for regular-cooled samples did not extend to the Mn axis as it was found to contain layered−layered phase separation, which corroborates previous results.[4,15]

The single-phase cubic spinel region for regular-cooled samples was found to exist at lower Mn contents in every cobalt slice ternary when compared to the corresponding quenched single-phase region. This result was attributed to the oxygen deficiency of quenched samples that favored the formation of lower oxygen content structures during heating, such as cubic spinel or layered structures. This effect caused the quenched spinel region to extend to higher Mn contents than the corresponding regular-cooled region.

Contour plots of layered lattice parameters and calculated unit cell volume per MO_2 basis unit were constructed for the cubic spinel and layered-rocksalt single-phase regions of the regular-cooled 10% cobalt slice ternary. These contour plots indicated a strong negative relationship between Li content and the resulting unit cell volume of a given single-phase material, for each of the spinel, layered, and rocksalt structures. There was no discernible effect on the MO_2 cell volume when replacing Ni with Mn or vice versa in spinel or layered single-phase structures.

The complex coexistence region existing within the Li−Ni−Mn−Co−O pseudoquaternary system was briefly investigated by observing the fitted XRD patterns of quenched samples located in the coexistence region near the lower boundary to the spinel region of the 20% cobalt slice system. This coexistence region proved extremely complex though, with the fact that tie-lines can terminate at any point on a surface making it impossible to determine the end points of a tie-line with only a few lattice parameters. As such, we focused on identifying the boundaries of the single-phase regions.

Most importantly to the lithium-ion battery community, this study determines the boundaries of the layered region within this system, which includes the Li-rich oxides of intense interest as next-generation positive electrode materials. This is a significant contribution as it identifies the composition ranges that the community should focus on in order to find the Li−Co−Mn−Ni−O composition which minimizes the negative characteristics that are currently preventing the commercialization of the Li-rich layered materials.

■ ASSOCIATED CONTENT

Supporting Information

List of hexagonal lattice parameters retrieved from the XRD fits for all single-phase layered compositions in this work and list of cubic lattice parameters retrieved from the XRD fits of all single-phase spinel compositions in this work.The Supporting

DOI: 10.1021/acscombsci.5b00048
ACS Comb. Sci. 2015, 17, 381−391

Information is available free of charge on the ACS Publications website at DOI: 10.1021/acscombsci.5b00048.

AUTHOR INFORMATION

Corresponding Author

*E-mail: jeff.dahn@dal.ca. Voice: 1 (902) 494 2991.

Present Addresses

Colby R. Brown: RIKEN Research Institute, 2-1 Hirosawa, Wako-shi, Saitama, 351-0198, Japan.

Eric McCalla: Collège de France, Chimie du Solide et de l'Energie, FRE 3677, 11 place Marcelin Berthelot, 75231 Paris Cedex 05, France.

Author Contributions

The manuscript was written through contributions of all authors. All authors have given approval to the final version of the manuscript.

Notes

The authors declare no competing financial interest.

REFERENCES

(1) Kim, T.; Park, J.; Change, S. K.; Choi, S.; Ryu, J. H.; Song, H. The Current Move of Lithium Ion Batteries Towards the Next Phase. *Adv. Energy Mater.* **2012**, *2* (7), 860−872.

(2) Xu, B.; Qian, D.; Wang, Z.; Meng, Y. S. Recent Progress in Cathode Materials Research for Advanced Lithium Ion Batteries. *Mater. Sci. Eng.* **2012**, *73*, 51−65.

(3) Carey, G. H.; Dahn, J. R. Combinatorial Synthesis of Mixed Transition Metal Oxides for Lithium-Ion Batteries. *ACS Comb. Sci.* **2011**, *13* (2), 186−189.

(4) McCalla, E. Consequences of Combinatorial Studies of Positive Electrodes for Li−ion Batteries. Ph.D. Thesis, Dalhousie University, Halifax, Nova Scotia, Canada, December 2013.

(5) McCalla, E.; Rowe, A. W.; Shunmugasundaram, R.; Dahn, J. R. Structural Study of the Li−Mn−Ni Oxide Pseudoternary System of Interest for Positive Electrodes of Li−Ion Batteries. *Chem. Mater.* **2013**, *25*, 989−999.

(6) McCalla, E.; Li, J.; Rowe, A. W.; Dahn, J. R. The Improved Electrochemistry of Single-Phase Layered Li−Mn−Ni−O Materials Over That of Layered-Layered Nano-Composites. *J. Electrochem. Soc.* **2014**, *161* (4), A606−A613.

(7) Ohzuku, T.; Makumura, Y. Layered Lithium Insertion Material of $LiCo_{1/3}Ni_{1/3}Mn_{1/3}O_2$ for Lithium-Ion Batteries. *Chem. Lett.* **2001**, *30* (7), 642−643.

(8) Zhang, X.; Jiang, W. J.; Mauger, A.; Qi, L.; Gendron, F.; Julien, C. M. Minimization of the Cation Mixing in $Li_{1+x}(NMC)_{1-x}O_2$ as Cathode Material. *J. Power Sources* **2010**, *195* (5), 1292−1301.

(9) He, P.; Wang, H.; Qi, L.; Osaka, T. Electrochemical Characteristics of Layered $LiNi_{1/3}Co_{1/3}Mn_{1/3}O_2$ and With Different Synthesis Conditions. *J. Power Sources* **2006**, *160* (1), 627−632.

(10) Shunmugasundaram, R.; Arumugam, R. S.; Dahn, J. R. High Capacity Li-Rich Positive Electrode Materials with Reduced First-Cycle Irreversible Capacity Loss. *Chem. Mater.* **2015**, DOI: 10.1021/cm504583y.

(11) Bettge, M.; Li, Y.; Gallagher, K.; Zhu, Y.; Wu, Q.; Lu, W.; Bloom, I.; Abraham, D. P. Voltage Fade of Layered Oxides: Its Measurement and Impact on Energy Density. *J. Electrochem. Soc.* **2013**, *160* (11), A2046−A2055.

(12) Cho, Y.; Lee, S.; Lee, Y.; Hong, T.; Cho, J. Spinel-Layered Core−Shell Cathode Materials for Li−Ion Batteries. *Adv. Energy Mater.* **2011**, *1* (5), 821−828.

(13) Brown, C. R.; McCalla, E.; Dahn, J. R. Analysis of the Cubic Spinel Region of the Li−Co−Mn Oxide Pseudo-ternary System. *Solid State Ionics* **2013**, *253*, 234−238.

(14) McCalla, E.; Carey, G. H.; Dahn, J. R. Lithium Loss Mechanisms During Synthesis of Layered $Li_xNi_{2-x}O_2$ for Lithium Ion Batteries. *Solid State Ionics* **2012**, *219*, 11−19.

(15) McCalla, E.; Lowartz, C. M.; Brown, C. R.; Dahn, J. R. Formation of Layered−Layered Composites in the Li−Co−Mn Oxide Pseudoternary System During Slow Cooling. *Chem. Mater.* **2013**, *25*, 912−918.

(16) Li, W.; Reimers, J. N.; Dahn, J. R. Crystal Structure of $Li_xNi_{2-x}O_2$ and a Lattice-Gas Model For the Order−Disorder Transition. *Phys. Rev. B* **1992**, *13* (3), 3236−3246.

DOI: 10.1021/acscombsci.5b00048
ACS Comb. Sci. 2015, 17, 381−391